East Antarctic sources of extensive Lower–Middle Ordovician turbidites in the Lachlan Orogen, of the southern Tasmanides, eastern Australia

R. A. Glen[a], I. C. W. Fitzsimons[b], W. L. Griffin[a,c] and A. Saeed[a]

[a] National Key Centre for Geochemical Evolution and Metallogeny of Continents, Department of Earth & Planetary Sciences, Macquarie University, Sydney, NSW 2109, Australia

[b] Department of Applied Geology and the Institute for Geoscience Research, Western Australian School of Mines, Curtin University, GPO Box U1987, Perth, WA 6845, Australia

[c] ARC Centre of Excellence for Core to Crust Fluid Systems (CCFS), Department of Earth & Planetary Sciences, Macquarie University, Sydney, NSW 2109, Australia

SUPPLEMENTARY PAPERS

Copies of Supplementary Papers may be obtained from the Geological Society of Australia's website (www.gsa.org.au), the Australian Journal of Earth Sciences website (www.ajes.com.au) or from the National Library of Australia's Pandora archive (http://nla.gov.au/nla.arc-25194).

Supplementary Papers

Appendix 1 $T_{DM}c$ plots for different clusters.

Appendix 2. Analytical procedures and methods.

Appendix 3. The basis for the model age data in Table 2, where they are shown as peak ages with 1 σ spread.

Appendix 4. Use of terms late Panafrican and late Grenvillian). In order not to break up the whole Grenvillian population (ca 950–1250 Ma), we use $^{206}Pb/^{238}U$ ages used for zircon ages up to 1250 Ma. For older ages we use $^{207}Pb/^{206}Pb$.

Appendix 5. Summary of detrital zircon age patterns of sedimentary sequences 2, 3 and 4 of the Ross Orogen.

Appendix 6. U–Pb data. (Excel file)

Appendix 7. ε_{Hf} data. (Excel file)

Appendix 1 Additional information on zircon populations

## *06E1 Scropes Range Formation (Figure 5)*

The lone, zircon grain at 438 Ma has an εHf value of +10 and geochemistry consistent with growth from high-silica granitoid magma (Figure 5g). This grain is younger than the host rock and may possibly represent metamorphic zircon growth, rather than Pb loss, since its εHf is higher than any other analysed grain.

Figure 5i in Appendix 1 is a mean of four out of five youngest grains of 514 ± 5 Ma (95% confidence, MSWD = 0.72, probability 0.54).

Figure 5j in Appendix 1 is a mean of the oldest 10 grains in a 12 grain spread of 562 Ma ± 3 Ma (95% confidence, MSWD = 0.99, probability 0.44).

Figure 5k in Appendix 1 is a mean of five grains of 590 ± 5 Ma (95% confidence, MSWD = 0.42, probability 0.79).

Figure 5l in Appendix 1 is a mean of 14 grains of 1183 ± 8 Ma (95% confidence, MSWD = 1.4, probability 0.15).
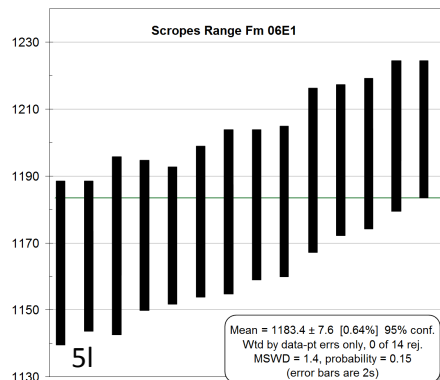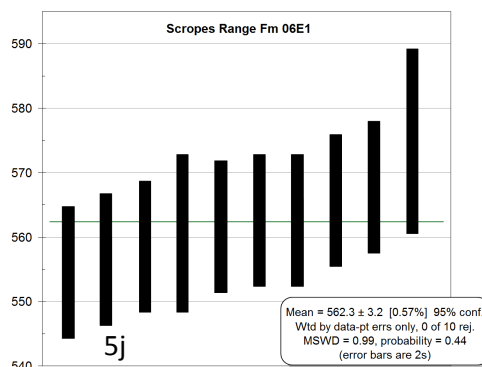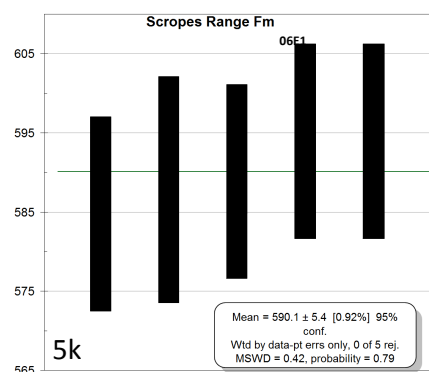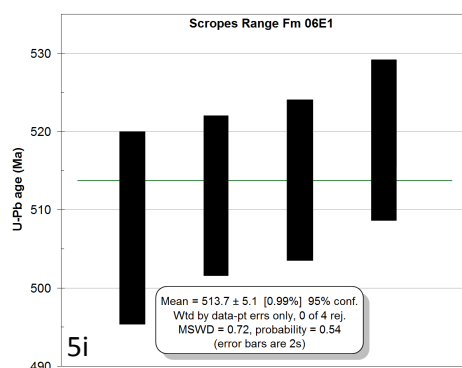
606 Yandaminta Quartzite (Figure 6)

Figure 6i in Appendix 1 is a mean of five
grains of 495 ± 5 Ma (95 % confidence,
MSWD = 0.78, probability 0.54).

Figure 6j is a mean from six grains of 514 ± 5
Ma (95 % confidence, MSWD = 0.31,
probability 0.91).

Figure 6k is a mean from seven grains
between *ca* 1160–1190 Ma of 1176 ± 7
Ma (95 % confidence, MSWD = 1.6,
probability 0.14).

Yandaminta Qtzite 606

Mean = 495 ± 5 [1%] 95% conf.
Wtd by data-pt errs only, 0 of 5 rej.
MSWD = 0.78, probability = 0.54
(error bars are 2σ)

6i

Yandaminta Qtzite 606

Mean = 514 ± 5 [0.96%] 95% conf.
Wtd by data-pt errs only, 0 of 6 rej.
MSWD = 0.31, probability = 0.91
(error bars are 2σ)

6j

Yandaminta Qtzite 606

Mean = 1176.4±6.8 [0.58%] 95% conf.
Wtd by data-pt errs only, 0 of 7 rej.
MSWD = 1.6, probability = 0.14 (box heights are 2s)

6k
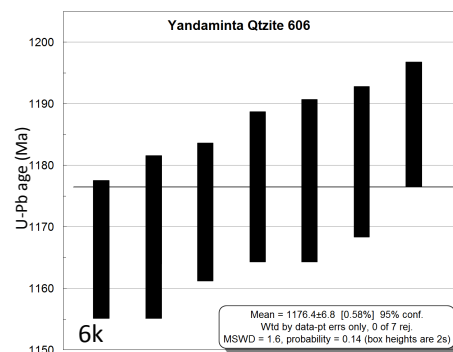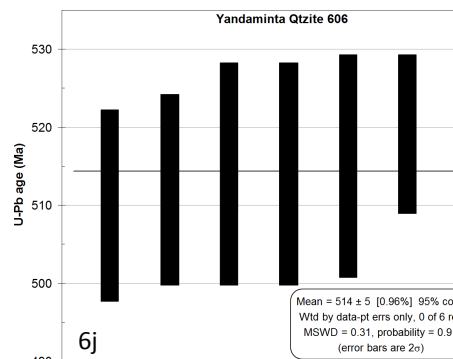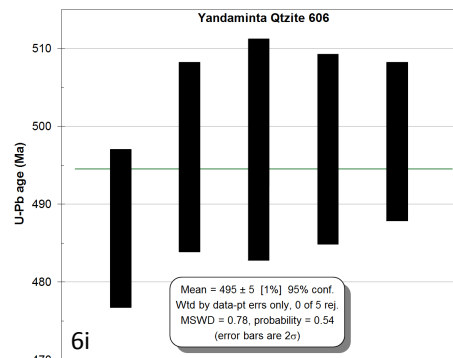
Ben2 Castlemaine Group (Figure 8)

Figure 8i is a mean of the five youngest grains of 487 ±
4 Ma (95 % confidence level, MSWD = 0.21,
probability = 0.93).

Figure 8j is a mean of four out of six grains of 1044 ±
10 Ma (95 % confidence level, MSWD = 0.77,
probability = 0.51).

Castlemaine Gp Ben 2

Mean = 487.2 ± 4.4 [0.90%] 95% conf.
Wtd by data-pt errs only, 0 of 5rej.
MSWD = 0.21, probability = 0.93
(error bars are 2σ)

8i

Castlemaine Gp Ben 2

Mean = 1044 ± 10 [0.96%] 95% conf.
Wtd by data-pts errs only, 0 of4 rej.
MSWD = 0.77, probability = 0.51
(error bars are 2σ)

8j
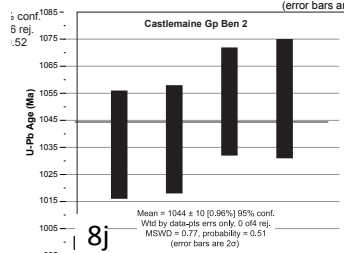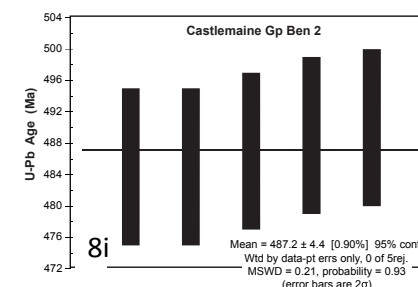
Ben5 Castlemaine Group (Figure 9)

Figure 9i shows a mean age from four youngest out of five grains (omitting the oldest) of 490 ± 5 Ma (95% confidence, MSWD = 0.87, probability = 0.46).

Figure 9j shows a mean age from all three grains between 1000-1040 Ma of 1015 ± 11 Ma (95% confidence, MSWD = 0.21, probability = 0.81).

Figure 9k shows a mean age from all three grains from *ca* 1050 to 1060 of 1062 ± 13 Ma (95% confidence, MSWD = 1.14, probability = 0.32).
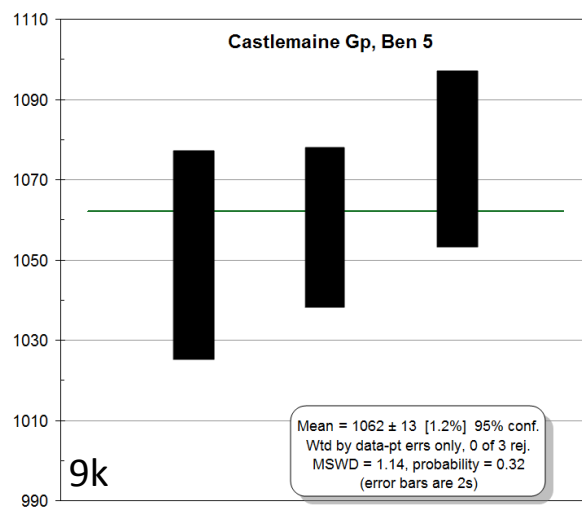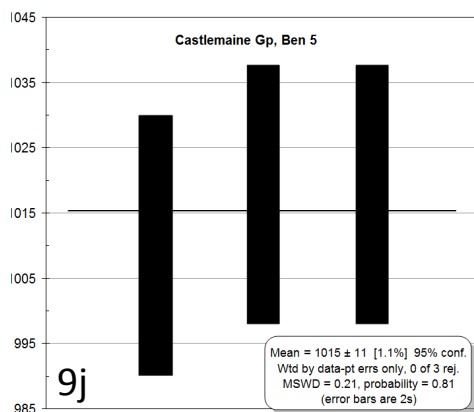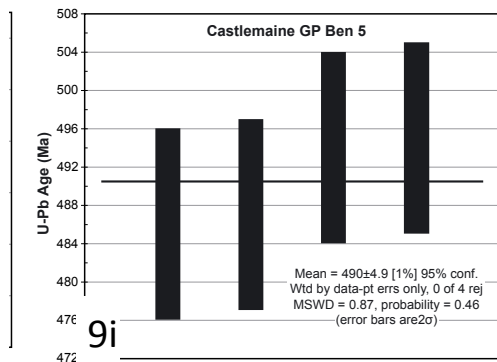
Cob1 Castlemaine Group

Figure 10i shows a mean age from four out of five older grains between ca 480–500 Ma of 493 ± 6 Ma (95% confidence, MSWD = 0.75, probability = 0.52).

Figure 10j shows a mean age from all 10 grains of 552 ± 3 Ma (95% confidence, MSWD = 0.77, probability = 0.64).

Figure 10k shows a mean age from all five grains between 1000–1040 Ma of 1078 ± 9 Ma (95% confidence, MSWD = 1.02, probability = 0.40).
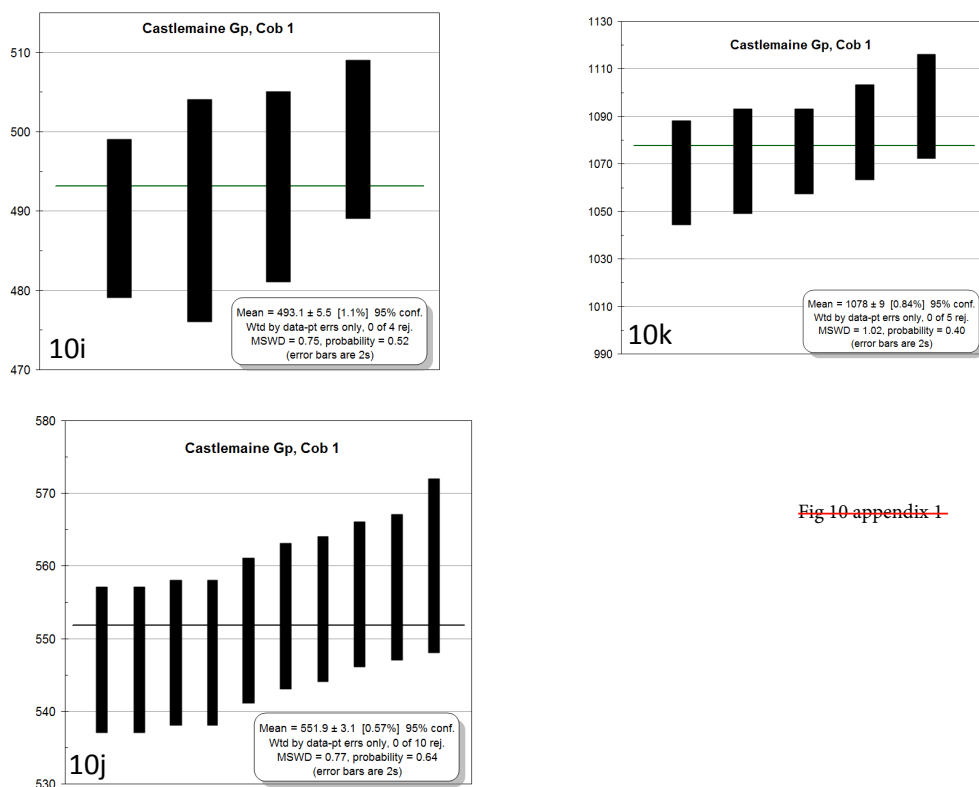

~~Fig 10 appendix 1~~

Te2 Girilambone Group

Figure 14i shows a mean age from all 13 grains of 555 ± 5 (95% confidence, MSWD = 0.66, probability = 0.62).

Figure 14j shows a mean age from all three grains of 1011 ± 11 (95% confidence, MSWD = 0.0033, probability = 0.997).
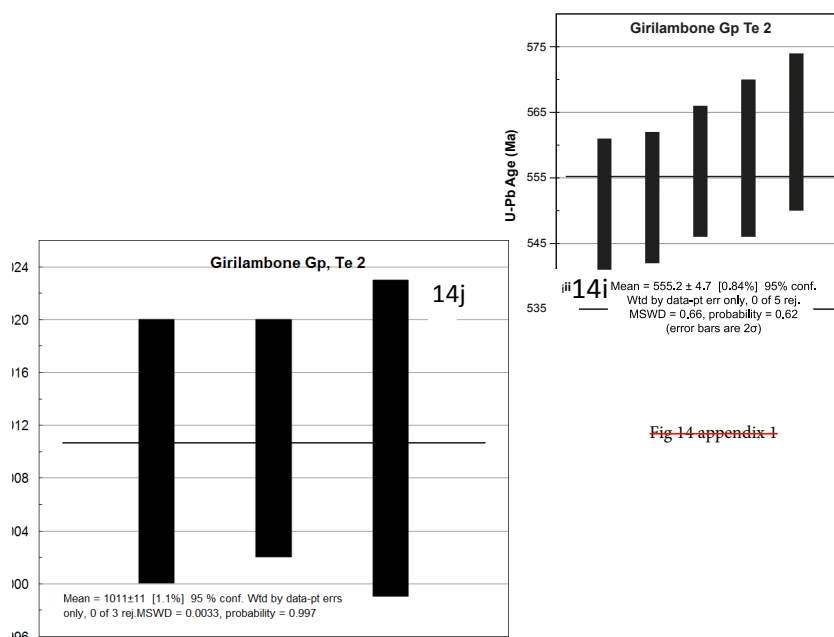
~~Fig 14 appendix 1~~

Oggyc1 Girilambone Group

Figure 15i shows a weighted mean age from all five grains of 491 ± 5 Ma (95% confidence level, MSWD = 1.04, probability = 0.38).

Figure 15j shows a weighted mean age from five out of six oldest grains of 1060 ± 9 Ma (95 % confidence level, MSWD = 0.85, probability = 0.51).

Figure 15k shows a weighted mean age from all three grains of 1115 ± 15 Ma (95% confidence level, MSWD = 0.55, probability = 0.58).
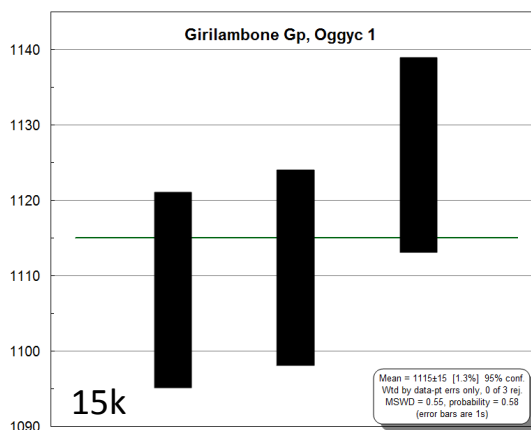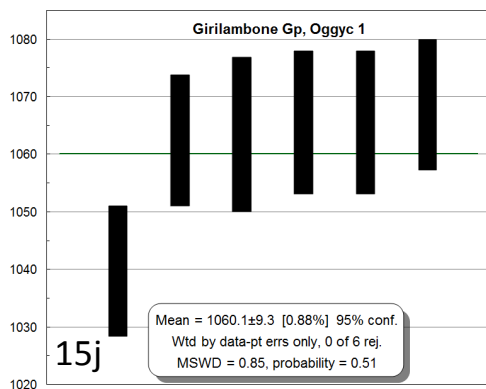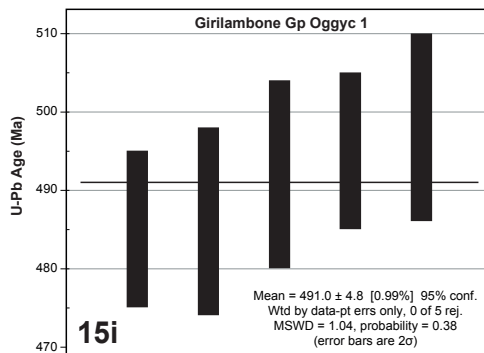
Mum1 Adaminaby Group

Figure 20g shows a weighted mean age from four grains of 579 ± 7 Ma (95% confidence level, MSWD = 0.15, probability = 0.93).

Figure 20h shows a weighted mean age from four grains of 1044 ± 1 Ma (95% confidence level, MSWD = 0.78, probability = 0.51).

20g
Adaminaby Gp Mum 1
Mean = 578.5 ± 6.6 [1.1%] 2σ
Wtd by data-pts errs only, 0 of 4 rej.
MSWD = 0.15, probability = 0.93

20h
Adaminaby Gp Mum 1
Mean =1044± 1.2 [1.1%] 2σ
Wtd by data-pts errs only, 0 of 4 rej.
MSWD = 0.78, probability = 0.51
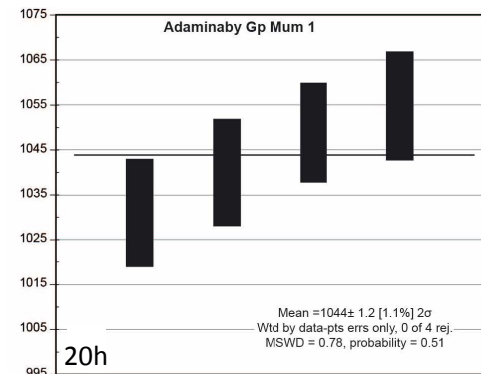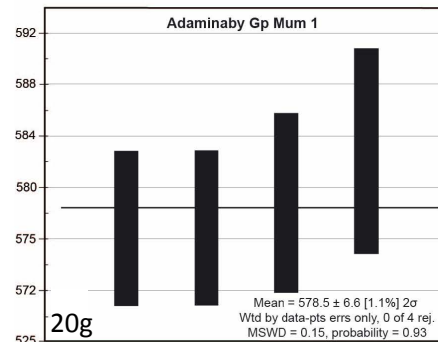
Bun8 Adaminaby Group

Figure 21i shows a weighted mean age from six grains of 542 ± 5 Ma (95% confidence level, MSWD = 0.21, probability = 0.96).

Figure 21j shows a weighted mean age from four grains of 1024 ± 11 Ma (95% confidence level, MSWD = 0.25, probability = 0.86).

21i
Adaminaby Gp Bun8
Mean = 541.7 ± 4.9 [0.91%] 95% conf.
Wtd by data-pt errs only, 0 of 6 rej.
MSWD = 0.21, probability = 0.96
(error bars are 2s)

21j
Adaminaby Gp Bun8
Mean = 1024 ± 11 [1.1%] 95% conf.
Wtd by data-pt errs only, 0 of 4 rej.
MSWD = 0.25, probability = 0.86
(error bars are 2s)
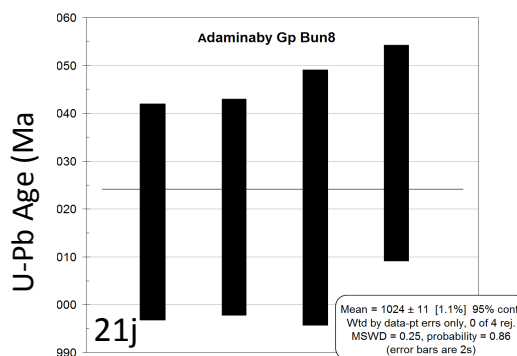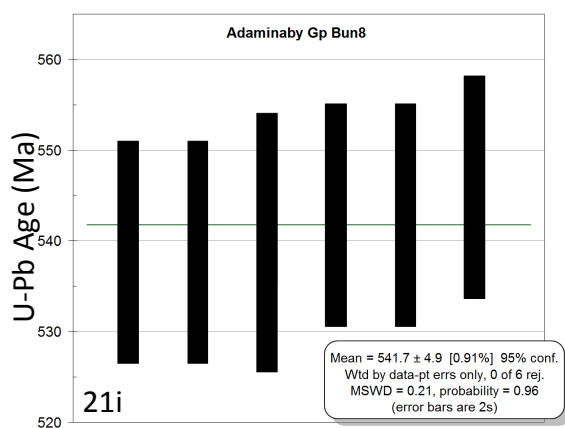
Appendix 2: Analytical procedures and methods

The mineral composition of selected sandstone samples was determined using the QEMSCAN technology system, invented by CSIRO and now owned by FEI. The system uses back-scattered electron imaging to map and locate individual grains. It then samples multiple points within each grain to produce an energy-dispersive X-ray spectrum that is analysed to give the chemical composition of the grain itself.

For zircon analysis, all samples except three were crushed at Geotrack International (Melbourne). Mum1 and Mwb1 and TrittonNE were disintegrated using the selFrag (electrostatic disaggregation) approach. Zircons were extracted from the resulting heavy mineral separates. U–Pb isotope analyses for individual grains were performed using a HP 7500 quadrupole ICP-MS, attached to a New Wave/Merchantek UP213 laser ablation system ($\varepsilon\lambda$ = 213 nm) with ablation carried out in He. This was done at GEMOC, Macquarie University, Sydney. Sample and analytical procedures have been described in detail by Belousova *et al.* (2002), Griffin *et al.* (2004) and Jackson *et al.* (2004). U–Pb ages were calculated from the raw signal data using the on-line software package GLITTER (www.mq.edu.au/GEMOC; Griffin *et al.* 2008); the common-lead correction of Andersen (2002) was used, but few grains required any common-Pb correction, and those requiring >10% correction were rejected. Concordia diagrams, weighted means and probability density distribution plots were generated using Isoplot (versions 3.0 and 3.2) software (Ludwig 2003). Samples were analysed in "runs" of 16 analyses, which include 12 unknown points, bracketed beginning and end by pairs of analyses of the GEMOC GJ-1 zircon standard. Two other well-characterised zircons, 91500 (Wiedenbeck *et al.* 1995) and Mud Tank (Black & Gulson 1978), were analysed frequently as an independent control on reproducibility and instrument stability. Analyses are included in Table 1. Age measurements are quoted in terms of errors of 1 sigma, with weighted means quoted at 95% confidence. Error bars in age plots are at 1 or 2 sigma as indicated. $^{206}Pb/^{238}U$ ages are used for zircon ages up to 1250 Ma, in order to treat 950–1200 Ma populations as a whole. For older ages we have used $^{207}Pb/^{206}Pb$ ages. We used cathodoluminescence (CL) microscopy and back-scattered electron (BSE) imaging on the electron microprobe (EMP) to image the internal features of zircon grains.

Our interpretation of source magmas from which the zircons crystallised is based on trace element geochemical analysis of zircon grains following the methods of Belousova *et al.* (2002). Five magma types are present: granitoids <65% SiO_2 (which we shorten to low-silica); granitoids with 70–75% SiO_2 (which we shorten to high-silica); mafic, alkaline, and rarely syenitic.

Not all zircons analysed for U–Pb were analysed for Lu–Hf. Hf-isotope analyses were carried out in-situ using a New Wave/Merchantek UP213 laser-ablation microprobe, attached to a Nu Plasma multi-collector ICPMS. The analyses were done with a beam diameter of *ca* 50 μm, a 5 Hz repetition rate, 30% iris, 0 expander and 90% power output. This resulted in total Hf signals of 1–6 x 10^{-11} A, depending on conditions and the Hf contents. Typical ablation times were 100–120 seconds, resulting in pits 40–60 μm deep. He carrier gas transported the ablated sample from the laser-ablation cell via a mixing chamber to the ICPMS torch. Aside from the use of this laser system, the analytical techniques are those described in detail by Griffin *et al.* (2000*)* and Griffin *et al.* (2004). Analytical standard MT-08 was used as a control sample, and analyses are included in Table 1.

The measured ^{176}Lu/^{177}Hf ratios are used to calculate initial ^{176}Hf/^{177}Hf ratios. The typical 2SE (Standard Error) uncertainty on a single analysis of ^{176}Lu/^{177}Hf is ± 1–2%, reflecting both analytical uncertainties and the intra-grain variation of Lu/Hf typically observed in zircons; at the Lu/Hf ratios considered here, this contributes an uncertainty of <0.1 ε_{Hf} f unit. For the calculation of ε_{Hf} values, we have adopted the chondritic values of Blichert-Toft *et al.* (1997). To calculate model ages (T_{DM}) based on a depleted-mantle source, we have adopted a model with (^{176}Hf/^{177}Hf)$_i$ = 0.279718 at 4.56 Ga and ^{176}Lu/^{177}Hf = 0.0384; this produces a present-day value of ^{176}Hf/^{177}Hf (0.28325), similar to that of average MORB (Griffin *et al.* 2000, 2004). There are currently three proposed values of the decay constant for ^{176}Lu: 1.93 x 10^{-11} yr^{-1} (Blichert-Toft *et al.* 1997); 1.865 x 10^{-11} yr^{-1} (Scherer *et al.* 2001); and 1.983 x 10^{-11} yr^{-1} (Bizzarro *et al. 2003)*; calculations using all three are provided in the data sheet (Table 1). ε_{Hf} values and model ages used in the figures have been calculated using the decay constant proposed by Blichert-Toft *et al.* (1997). T_{DM}c represents the time of separation of crustal rocks from the mantle and approximates to the age of crustal sources of the analysed zircon grains calculated from ε_{Hf} values. In this paper, T_{DM}c ages for each cluster of ε_{Hf} values for each sample are shown graphically in Appendix 3, and in Table 2. They approximate T_{DM}c ages in individual and comparison Hf plots, which were estimated graphically by projecting line-of-sight enveloping evolution lines through zircon clusters to the Depleted Mantle.

# Appendix 3: $T_{DM}c$ graphic plots for different samples and clusters.
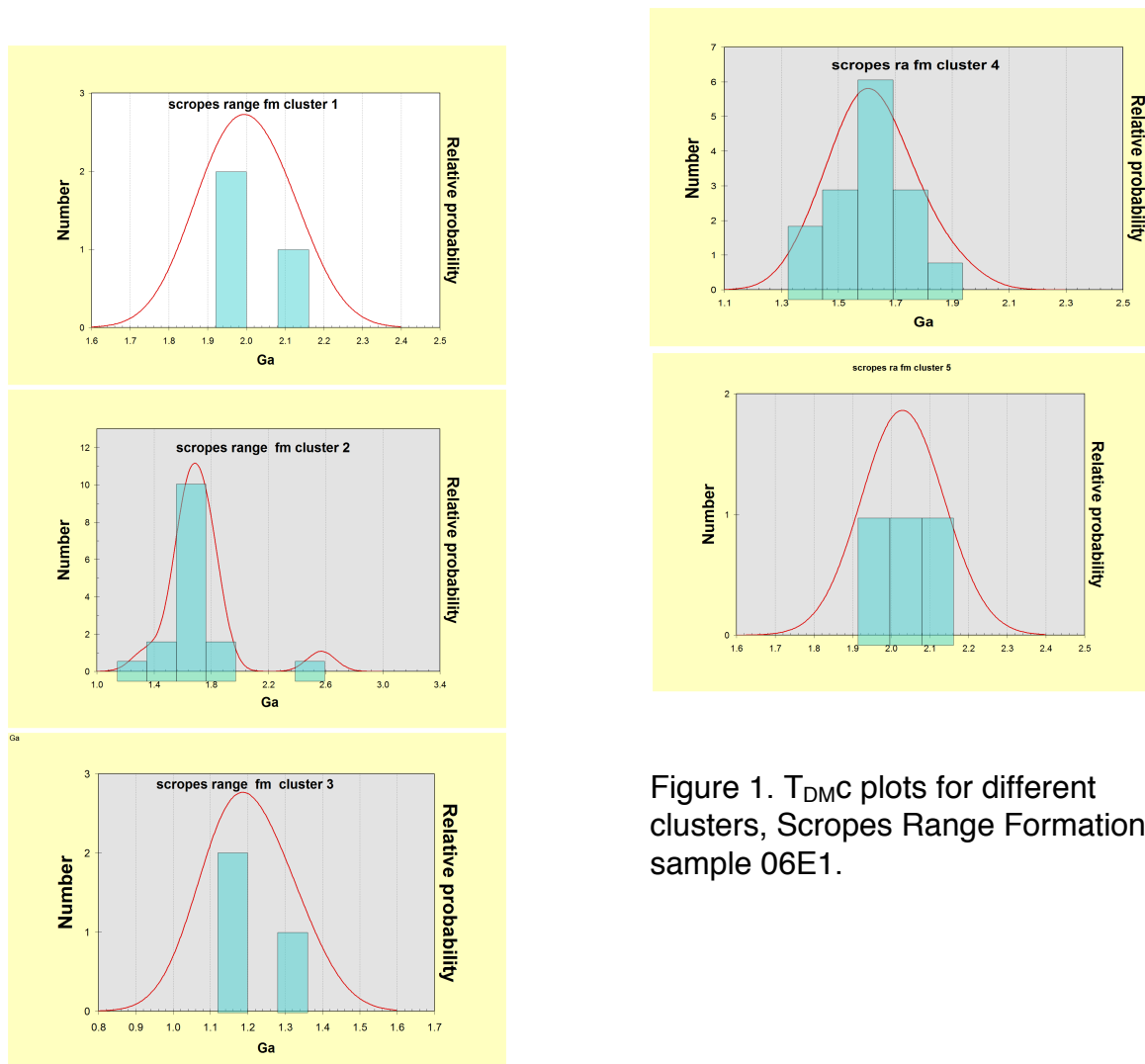
Figure 1. $T_{DM}c$ plots for different clusters, Scropes Range Formation, sample 06E1.
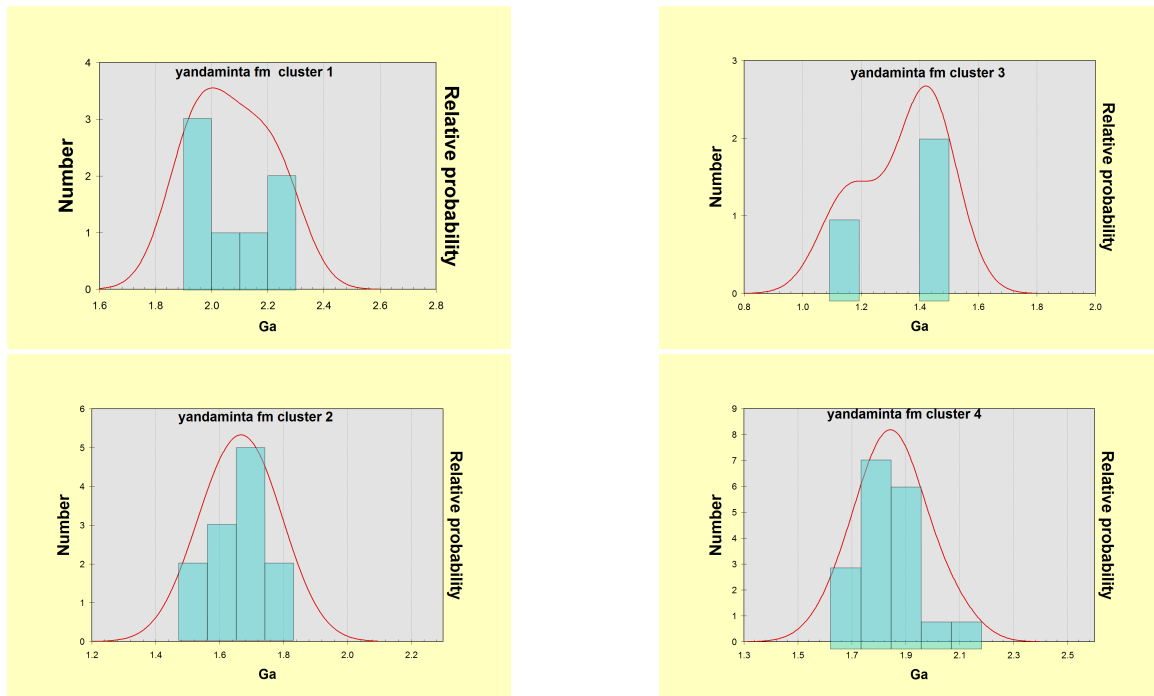
Figure 2. T$_{DM}$c plots for different clusters, Yandaminta Quartzite sample 606.
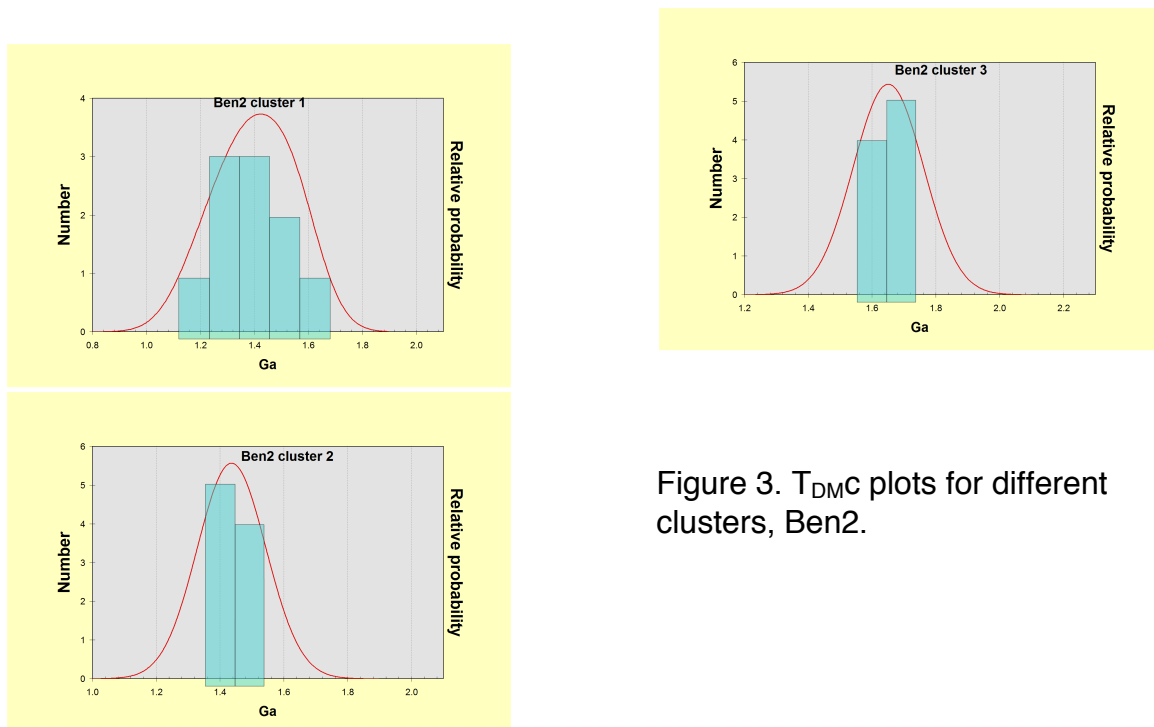
Figure 3. T$_{DM}$c plots for different clusters, Ben2.
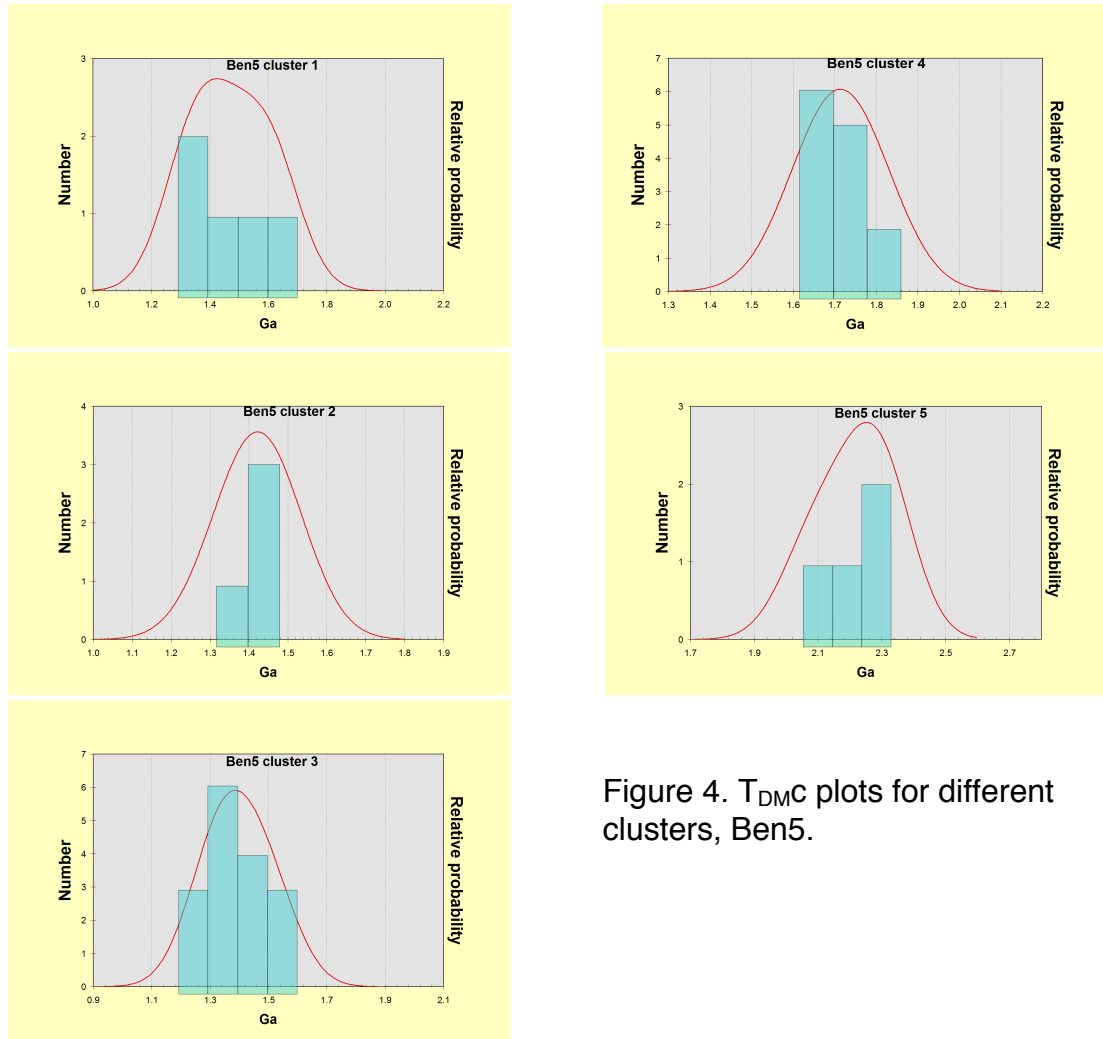
Figure 4. $T_{DM}c$ plots for different clusters, Ben5.
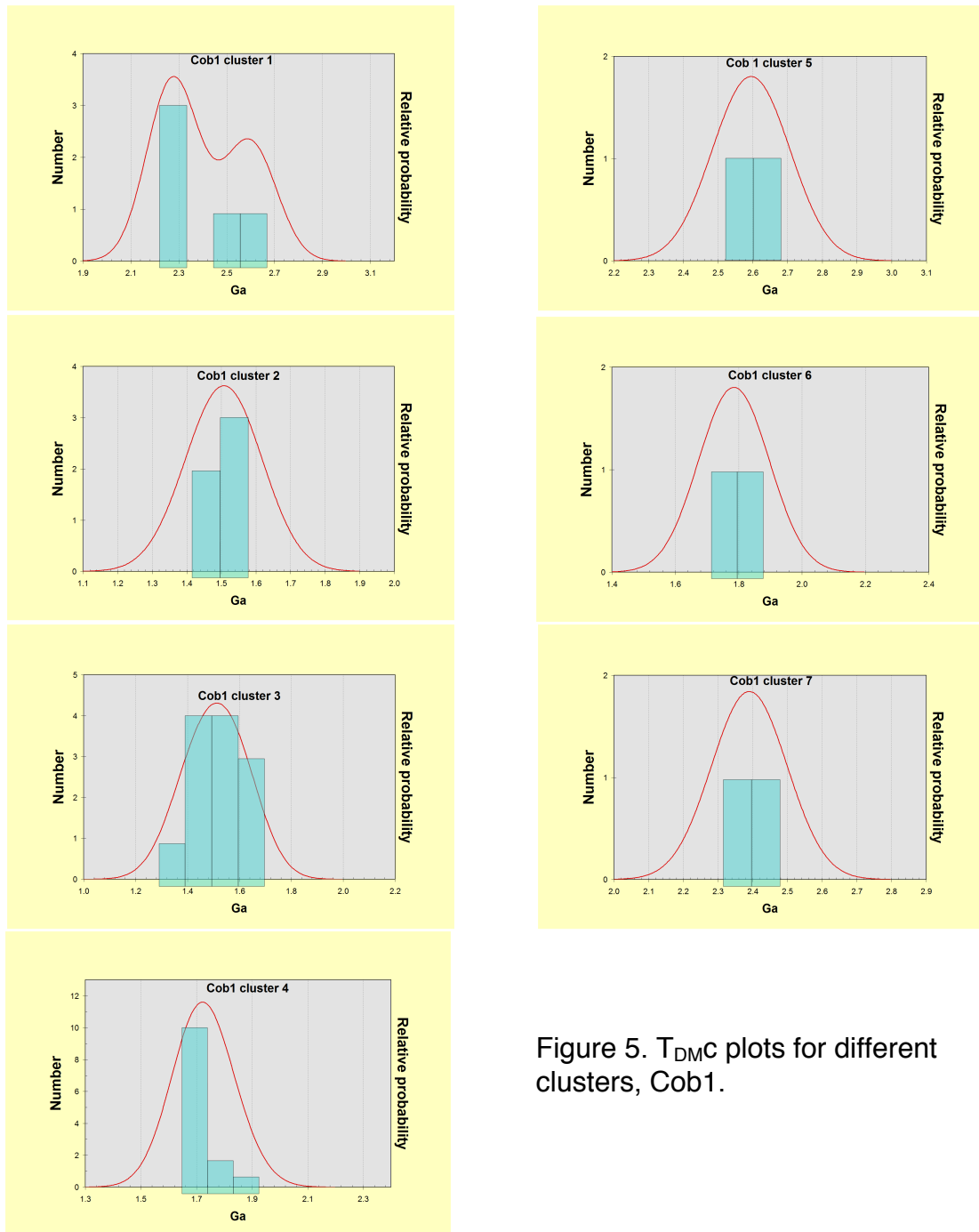
Figure 5. $T_{DM}c$ plots for different clusters, Cob1.
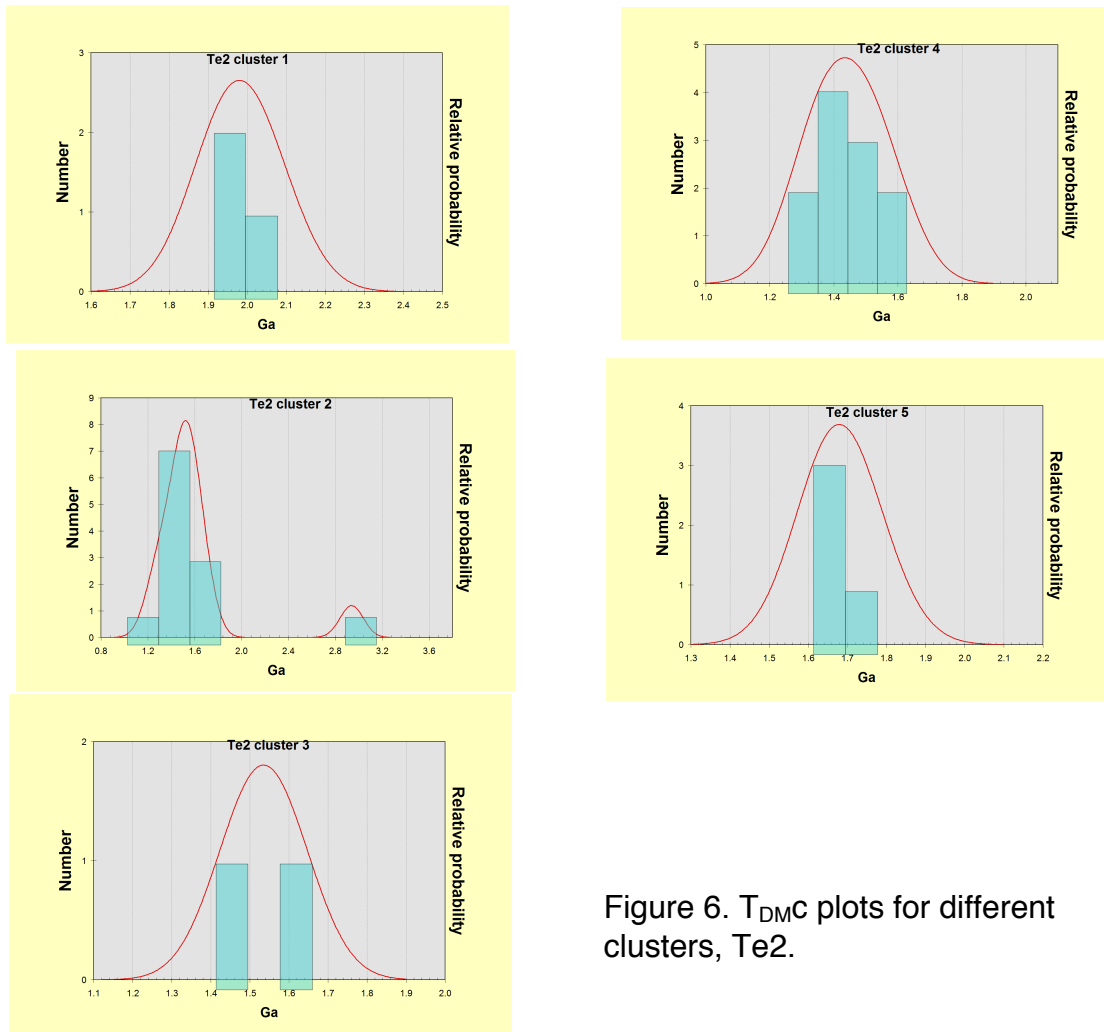
Figure 6. $T_{DM}c$ plots for different clusters, Te2.
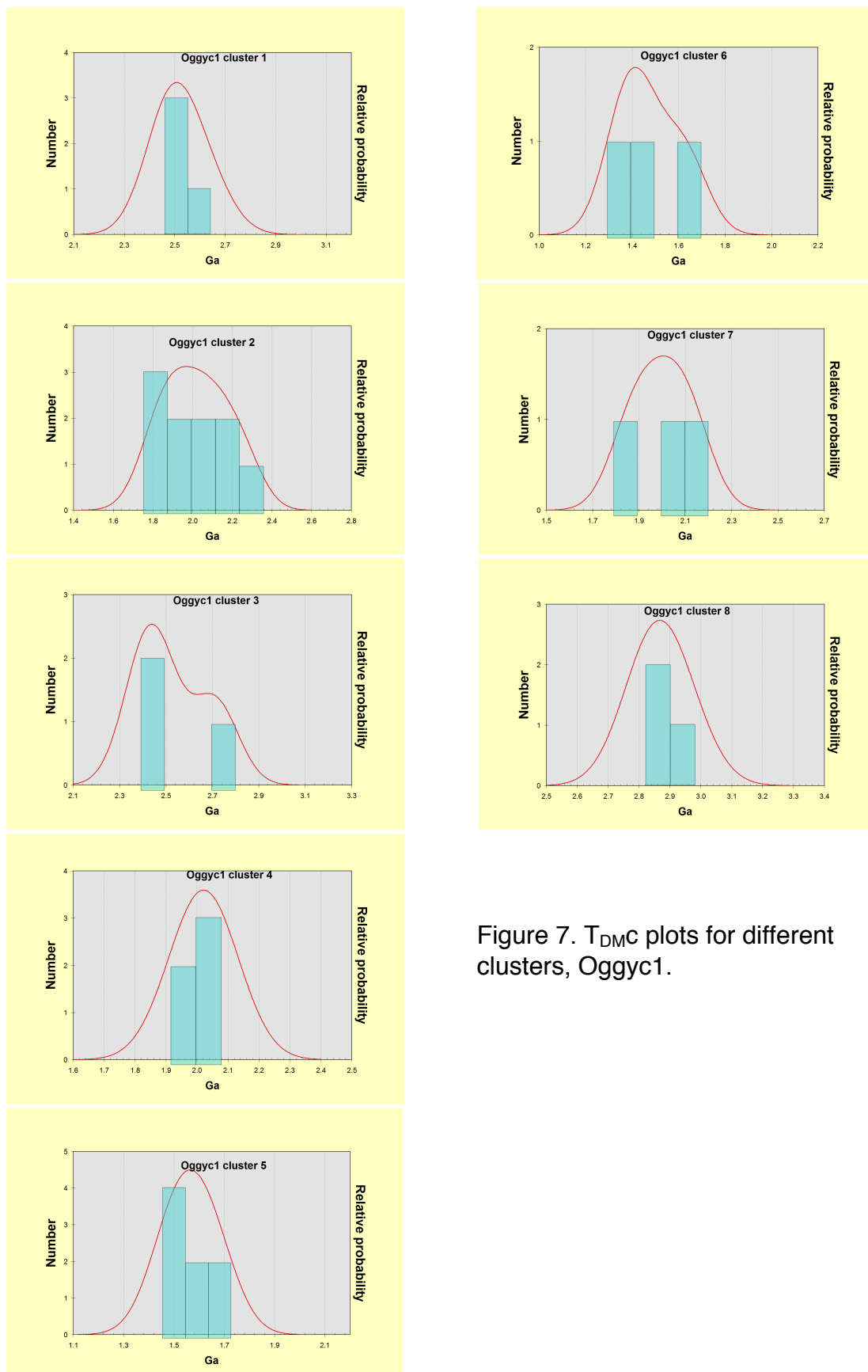
Figure 7. $T_{DM}c$ plots for different clusters, Oggyc1.

Figure 8. T_{DM}c plots for different clusters, Oww5.
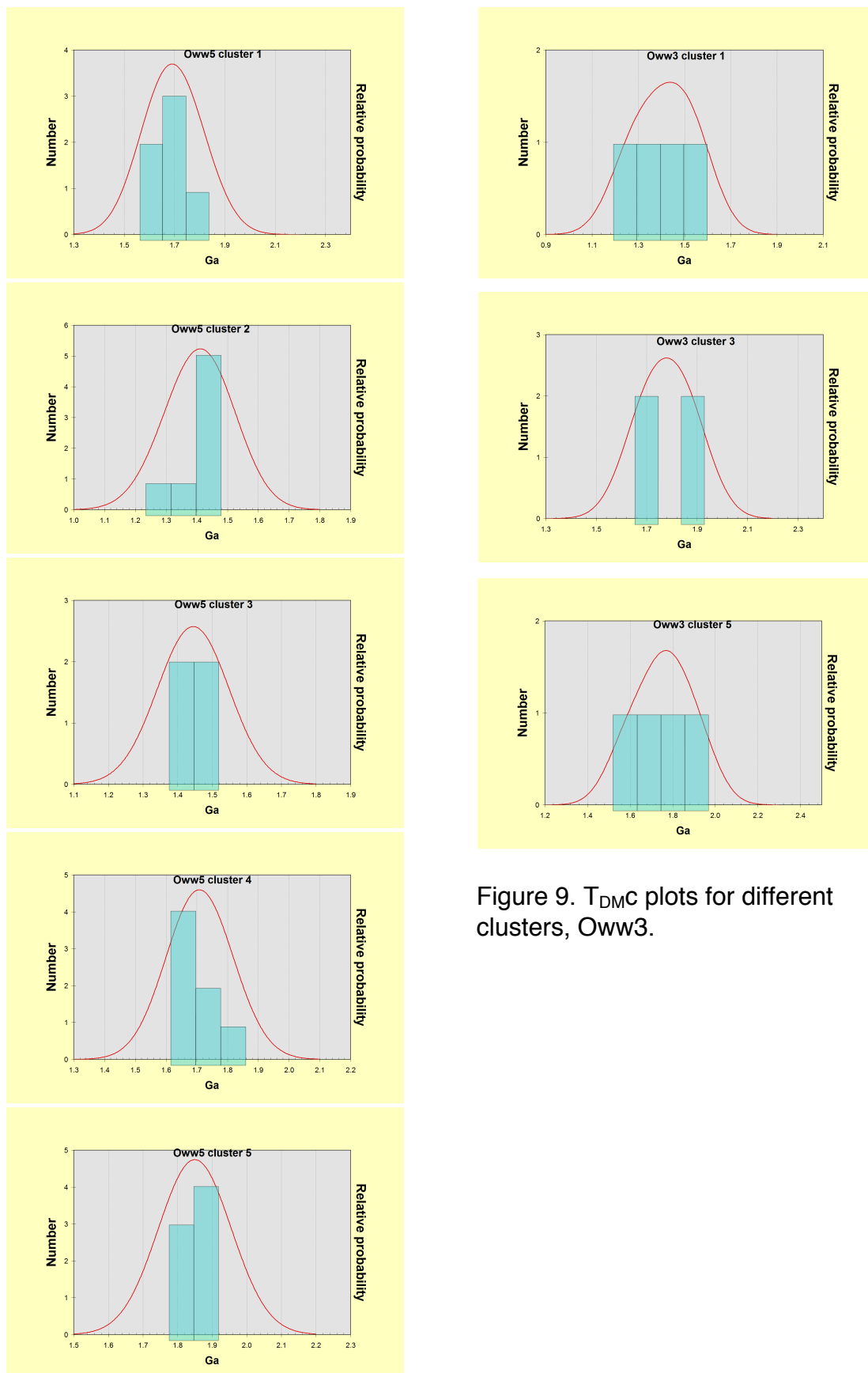
Figure 9. T_{DM}c plots for different clusters, Oww3.
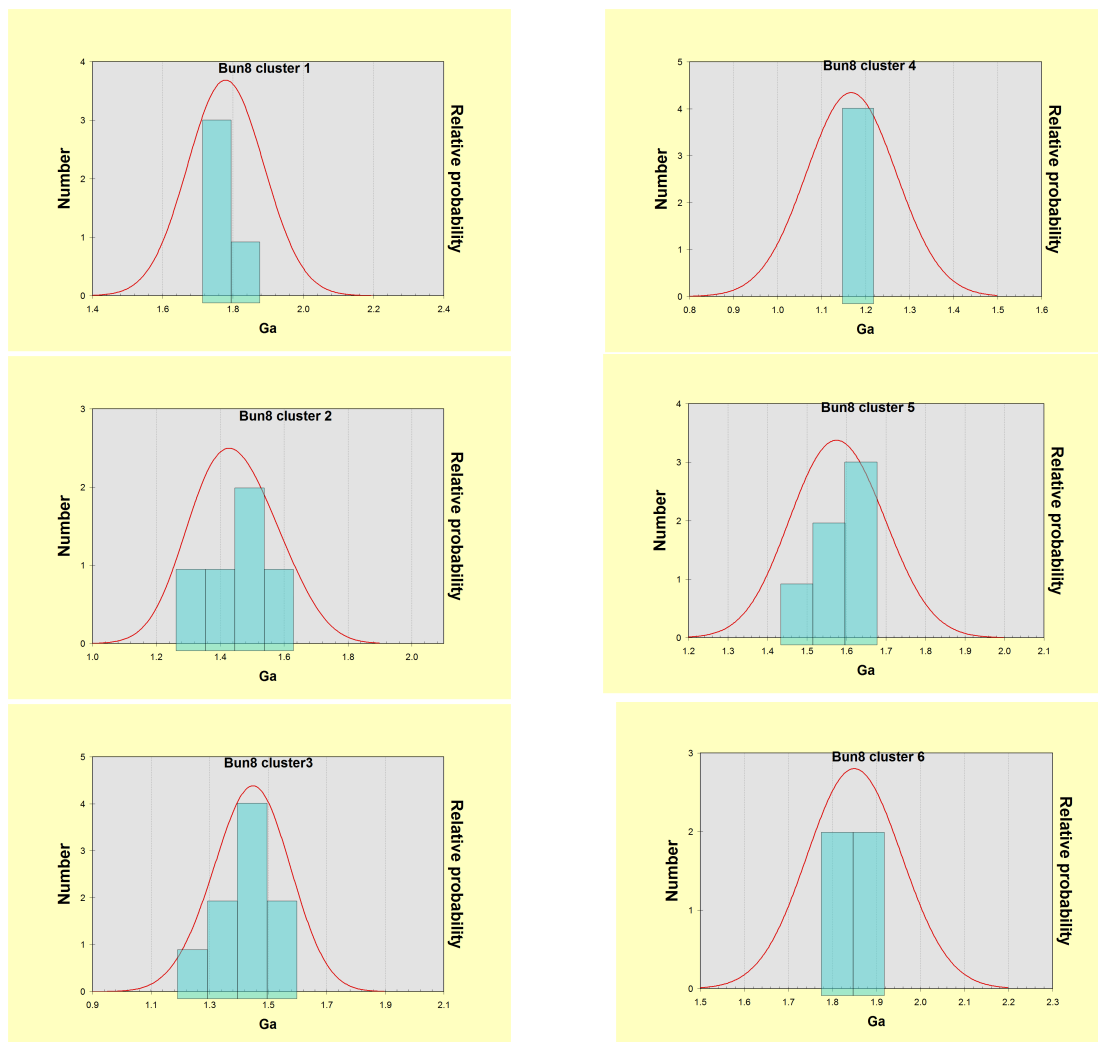
Figure 10. $T_{DM}c$ plots for different clusters, Bun8.
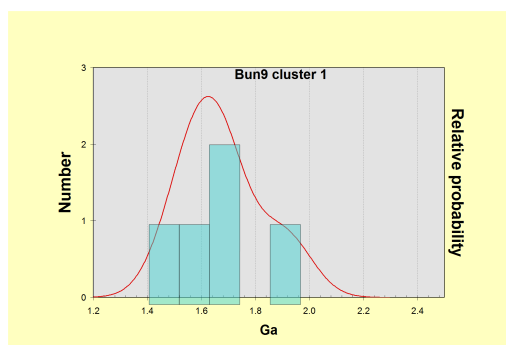
Figure 11. $T_{DM}c$ plot for different cluster 1, Bun9.
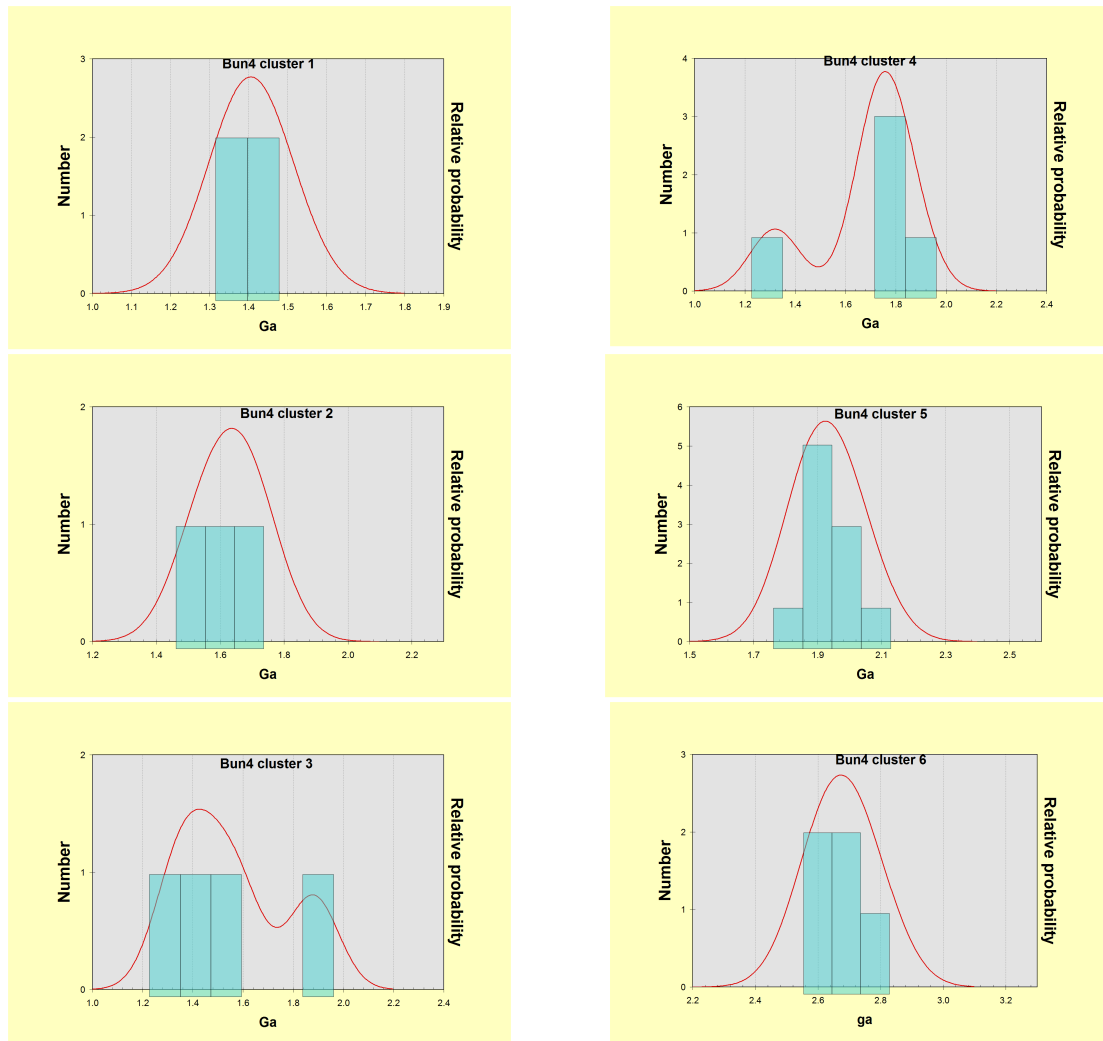
Figure 12. T$_{DM}$c plots for different clusters, Bun4.

Appendix 4: Terminology of zircon age populations

Previous workers, beginning with Ireland *et al.* (1998), have shown that the ages of detrital zircons in Ordovician turbidites of the Lachlan Orogen are dominated by a 500–600 Ma population, which they called Ross-Delamerian, and a 1100–1200 Ma population, which they called Grenvillean. Meert (2003) recognised a Panafrican event that he divided into two parts. The older East African Orogeny comprises: (i) assembly and accretionary phases between *ca* 660–750 Ma; (ii) a *ca* 620-650 Ma orogenic phase involving collision of eastern Africa with parts of Madagascar, India, Sri Lanka and east Antarctica; and (iii) post-collisional extension between 620 and 580 Ma. The younger part, between *ca* 530–550/570 Ma, was called the Kuunga Orogeny. Meert (2003) suggested it represented collision between Australia, parts of the previously assembled eastern African Orogen and parts of eastern Antarctica. Subsequently, Collins and Pisarevsky (2005) suggested that the term Kuunga Orogeny be restricted to events between *ca* 500-570 Ma. In an East Gondwana context, the Grenvillian metamorphism was subdivided by Fitzsimons (2000) into an oldest part (*ca* 1280–1330 and *ca* 1130–1200 Ma), resulting in the formation of the Albany-Fraser Orogen in western Australia; a youngest part (900–990 Ma) involving the Eastern Ghats of India and its Rayner Complex equivalent in Antarctica; and events of intermediate age (1030–1090 Ma) involving the Namqua-Natal province of southern Africa and its extension in Maud Belt of Antarctica, and coeval metamorphism in Pinjarra Orogen of Western Australia and its extensions in eastern Antarctica.

As discussed in the text, the two main populations of detrital zircons in our Ordovician turbidites fit with Panafrican (or Ross-Delamerian) and Grenvillian. Using plots of all the zircon ages in the Ordovician turbidites, we have calculated average upper and lower ranges of our two populations. Obviously in some turbidite sandstone the limit is a bit older or younger than the average. Calculated in this way, our average limits are 490–620 Ma and 950–1120 Ma. The first population overlaps with the later or younger part of the Panafrican Orogeny, and so we call those zircons late Panafrican. The secondary population overlaps with the two latest or youngest Grenvillian events and so is termed late Grenvillian.

Appendix 5: Summary of detrital zircon age patterns of sedimentary sequences 2, 3 and 4 of the Ross Orogen

Byrd Group (Sequences 3 and 4)

The syn-Ross deformation sedimentary sequence is best defined in the Central Transantarctic Mountains (lower Cambrian to Lower Ordovician Byrd Group). The lower Byrd Group of the Central Transantarctic Mountains includes carbonates and interbedded sandstones of Atdabanian-Botoman Shackleton Limestone that represents deposition on a deepening platform (Myrow *et al.,* 2002; Goodge *et al.,* 2004b). Corresponding ages are *ca* 521–513 Ma (Peng *et al.,* 2012). Detrital zircons from the lower sandstone sample SLB in the Shackleton Limestone display a main population of 1300–1700 Ma, and a secondary population of 1100–1250 Ma (Goodge *et al.,* 2004b), with small peaks at *ca* 970 and 1750–2000 Ma (see summary in Table 6). Detrital zircons have a similar age pattern to the Goldie Formation (upper Beardmore Group), with a dominant early Mesoproterozoic population (peak at 1515 Ma) and a smaller Grenvillian population (1050–1250 Ma, with peaks at 1135 and 1195 Ma) (Goodge *et al.,* 2004b).

The base of the overlying upper Byrd Group defines the base of sequence 4 composed mainly of Starshot Formation and Douglas Conglomerate (Figure 33). It is 513 Ma. Its upper age is poorly known, constrained only by small crosscutting intrusions dated at 504 and 494 Ma in two locations (Goodge *et al.,* 2004b). A possible minimum age as young as ?470 Ma (Goodge *et al.,* 2004b) is based on detrital zircon patterns from 8 samples that are dominated by a main population between *ca* 470–600 Ma, a secondary population of *ca* 930–1160 Ma, and smaller populations around 650–800 and over 1160 Ma (Goodge *et al.,* 2004b; Paulsen *et al.,* 2015) (Table 6). Deposition of the upper Byrd Group was assigned to the syn- to late-orogenic phases of the Ross Orogeny (Myrow *et al.,* 2002; Goodge *et al.,* 2004b).

The upper Byrd Group appears to have mixed sources. Angular to subangular zircons, including some dated at 547 ± 12 Ma, have been attributed to the now-eroded volcanic carapace of the continental margin arc (Goodge *et al.,* 2004b). Sandstone petrography and detrital muscovites (see below) suggest an additional older provenance that includes low-grade meta-sedimentary rock, granite and limestone either representing basement to the arc or from sediment recycling (Goodge *et al.,* 2004a, b).

Two samples of the Starshot Formation (upper Byrd Group) from the Queen Maud Mountains have multiple detrital zircon populations, with the dominant being Panafrican, with ages from 539–630 (RAM1) or 517–696 (RAM2). Populations from 632 to 796 (RAM1) and 859–891 (RAM2) are more common than the Grenvillian population of 983–1215 (RAM1) and 939–1297 (RAM2) (Paulsen *et al.,* 2015).

Detrital muscovite ages from sample RAM2 (sampled by Paulsen *et al.,* 2015) from the northern part of the Queen Maud Mountains showed a dominant population of 527–579 Ma (mainly 540–570 Ma) derived from probable mixtures of metamorphic and igneous sources. The next two highest samples of the upper Byrd Group (HRS and by inference DSG of Goodge *et al.,* 2004b, shown in Table 6 and Figure 34) are dominated by *ca* 490–750 Ma and 525–645 Ma populations respectively. Sample HRS is almost unimodal with only minor older grains, whereas sample DSG has near equal 810–825 Ma and 1000–1250 Ma populations as well as a less common one of 1400–1900 Ma (Goodge *et al.,* 2002) (Table 6). Sample DCS from the coeval, interfingering Douglas Conglomerate has almost a unimodal 500–600 Ma population (peak of 520 Ma) (Table 6). Stratigraphically higher up again, and inferred to be Ordovician in age by Goodge *et al.* (2004b), two samples of the Starshot Formation (USF and DIF) still possess the dominant Late Panafrican population (peaks of 520, and 510 & 555 Ma, Table 6), but also possess variable 900–1250 Ma (Grenvillian) populations (Goodge *et al.,* 2002, 2004b) (Table 6).

Liv Group and Patuxent Formation (Sequence 4)

In the Queen Maud Mountains south of the Shackleton Glacier, the Liv Group, with several formations, has been correlated with the Byrd Group (Paulsen *et al.,* 2015). The Wyatt and Ackerman formations are the oldest dated constituents, containing 526 and 524 Ma volcanics (cited in the main text). The Taylor Formation is one of the youngest, containing a 505 Ma rhyolite (see main text). It is joined by the Fairweather Formation (with a unimodal zircon peak of 506 Ma), and the Greenlee Formation with a unimodal zircon peak of 503 Ma, both probably reflecting adjacent volcanism (Paulsen *et al.,* 2015) (Table 6). Three samples from the Liv Group in the Queen Maud Mountains display unimodal or near unimodal age peaks of 529, 506 and 503 Ma.

In the Pensacola Mountains, the Patuxent Formation (with its main population of 500–620 Ma and secondary population of *ca* 900–1200 Ma) is correlated with the upper part of the Byrd Group, and inferred to be late Cambrian to Ordovician (Goodge *et al.,* 2004b) or middle to late Cambrian (Curtis *et al.,* 2004). The Patuxent Formation contains mafic–felsic volcanic rocks and sills that are probable correlatives of the Gambacorta Formation, with an age of *ca* 501 ± 3 Ma (Millar & Storey 1995). The Gorecki Felsite Member in the Patuxent Formation was dated at *ca* 500 ± 8 Ma, while basaltic lavas and sills have transitional MORB-like geochemistry (Millar and Storey, 1995) (Table 6). These two relations suggest interfingering relations (e.g. Rowell *et al.,* 2001).

Sequences 2 and 3

Sample KHF from the Hobbs Formation in the Skelton Group was dated by Goodge *et al.,* (2004b), although they attributed it to the Koettlitz Group, a term which has been largely been abandoned (Cook and Craw, 2001). This sample is dominated (56%), by *ca* 1000–

1150 Ma detrital zircons (peaks at 1080>1180>1000 Ma), with a secondary population of 500–650 Ma, containing a 675 Ma peak inferred to be derived from coeval rift-related volcanism (Table 6). Goodge *et al.* (2004b) also noted that apart from its 675 Ma peak, detrital ages in their sample were comparable with Goldie Formation rocks of the upper Beardmore Group and lower Byrd Group rocks of Central Transantarctic Mountains.

The Beardmore Group (Sequence 2) comprises the older Cobham Formation (*ca* 675–690 Ma) and the younger Goldie Formation (*ca* ?550–675 Ma), the latter constrained in part by the 668 Ma Golden Plateau Gabbro (Goodge *et al.,* 2002, 2004b; Myrow *et al.,* 2002). In both formations, the dominant detrital zircon population is *ca* 1400–1900 Ma with some older (*ca* 2500–3000 Ma) and younger (*ca* 1100–1300 Ma) grains. The youngest weighted mean detrital ages are 1096 to 1174 Ma, much older than the inferred Neoproterozoic depositional age range of *ca* 690–?550 Ma (Goodge *et al.,* 2002, 2004b) (Table 6). The Skelton Group, which includes the Hobbs Formation, consists of both weakly and strongly metamorphosed units (with the latter previously differentiated as the Koettlitz Group; Cook and Craw, 2001). The age of the Skelton Group is constrained by *ca* 650 Ma rift volcanics (Cooper *et al.,* 2011, and see above) and by metamorphism beginning at *ca* 615 Ma (Hagen-Peter *et al.,* 2016). The best age range is 615–675 Ma, suggesting overlap with the Beardmore Group. The Skelton Group contains a dominant Grenvillian detrital zircon population of *ca* 900–1300 Ma (Cooper *et al.,* 2011; Wysoczanski and Allibone, 2004; Stump *et al.,* 2007). Both Cooper *et al.* (2011) and Stump *et al.* (2007) recorded a smaller detrital zircon population at *ca* 630–900 Ma (absent from the Dry Valleys samples of Wysoczanski and Allibone, 2004). A variable 1500–2000 Ma population was recorded by Cooper *et al.* (2011). Small numbers of grains 2000–2500 Ma were also recorded by Stump *et al.* (2007*).*

In the Queen Maud Mountains, sedimentary units traditionally assigned to the Beardmore Group include the La Gorce and Duncan formations. The La Gorce Formation was deformed before intrusion of volcanics of the 526 Ma, sequence 4 Wyatt Formation of the Liv Group (Stump, 1995; Rowell *et al.,* 2001). Its age is poorly controlled. Curtis *et al.* (2004) suggested a stratigraphic base at ?550 Ma and a top at ?537 Ma, implying a younger age than the Beadmore Group. Two samples dated by Stump *et al.* (2007) showed approximately equal populations between *ca* 560 and 700 Ma and *ca* 1000–1200 Ma, with a few grains in one sample around 1250–1400 Ma, and only a few single grains older than that. The youngest age peaks in two samples are 581 and 618 Ma, with the youngest grains *ca* 560 Ma (Stump *et al.,* 2007). Uncertainty about the youngest depositional age in the Duncan Formation precludes firm correlation with the Goldie Formation in the Beardmore Group in the Central Transantarctic Mountains, but it may also be younger. Detrital zircons in the Duncan Formation define a major population between *ca* 550–755, a secondary population *ca* 950–

1170 Ma, a small population between *ca* 780–850 and only one grain (1282 Ma) older than 1 Ma (Paulsen *et al.,* 2015).

The Hannah Ridge Formation occurs in the Neptune Range, part of the Pensacola Mountains. A sample from the Hanna Ridge Formation, correlated with the lower part of the Byrd Group has subequal 550–700 Ma and 1000–1200 Ma populations (Goodge *et al.,* 2004b) (Table 6).

The best stratigraphic constraints are: i) the intrusive 505 Ma Serpan Granite above the unit (Curtis *et al.,* 2004); ii) the overlying Nelson Limestone, with Botoman fossils (Rowell *et al.,* 2001); and iii) the 501 Ma volcanic Gambacorta Formation that overlies the limestone (Rowell *et al.,* 2001). The Hannah Ridge Formation does not have the young late Panafrican grains of the Patuxent Formation: its main detrital zircon population *is ca* 550–650 Ma, with the youngest grouping of 556 Ma, and its secondary population is *ca* 900–1200 Ma (Goodge *et al.,* 2004b).

Sequences in Northern Victoria Land

In northern Victoria Land, sedimentary units occur in the Wilson, Bowers and Robertson Bay terranes. Detrital zircon age data are available for two upper Neoproterozoic to Cambrian to ?lower Ordovician sedimentary units in the Wilson terrane: the Berg Group in the north and the Priestley Formation in the south, both metamorphosed to greenschist facies. The Berg Group has a dominant Panafrican (*ca* 500–700 Ma) population and a secondary Grenvillian (*ca* 1000–1200 Ma) population, with other grains from *ca* 800–900 Ma and large numbers of grains from 2030–>3000 Ma (Adams *et al.,* 2014) (Table 6). Detrital muscovite grains in the Berg Group have several dominant peaks between 530–600 Ma and smaller peaks between 750–1170 Ma (Henjes-Kunst, 2003). The youngest grains (511 and 519 Ma, Henjes-Kunst, 2003) are close to (overlap within error) the metamorphic overprint with a Rb–Sr age of 515 ± 11 Ma (Adams *et al.,* 2014) and have been thus potentially reset. The Priestley Formation was divided into two parts by Estrada *et al.,* (2016). Four samples from the older *ca* 590–560 Ma, part contained a dominant Grenvillian zircon population (900–1300 Ma) and a lesser Panafrican zircon population (within 550–700 Ma, with the youngest grains in two samples being 592 and 602 Ma) with 23% of grains lying within 1600–2500 Ma (Table 6). The upper part of the Priestley Formation according to Estrada *et al.* (2016), is *ca* 550–?532 Ma, and corresponds with the Priestley Formation sample dated by Adams *et al.,* (2014). That sample has a dominant zircon population of *ca* 900–1200 Ma, a secondary population of 450–700 Ma, plus large numbers of grains from 2000 to 3400 Ma (Adams *et al.,* 2014) (Table 6). The youngest mean age is 546 Ma, older than the Rb–Sr age of metamorphism of 512 Ma of Adams *et al.* (2014). From the Priestley Formation, Di Vincenzo *et al.* (2014) recorded single mica fusion ages mainly around 550–650 Ma (Table 6).

Northern Victoria Land also contains the middle–upper Cambrian strata of the Bowers Terrane and ?Cambrian–Ordovician strata of the Robertson Bay Terrane (see summary by Rocchi *et al.,* 2011). Samples of the Molar Group, Bowers Terrane have a main detrital zircon population of *ca* 490–670 (youngest grain 498 Ma, youngest component 545 Ma) and a secondary population of *ca* 950–1250 Ma (Adams *et al.,* 2014). Estrada *et al. (*2016) recorded a dominant population within a 900–1300 Ma bracket and a slightly less prominent one within a 495–700 Ma bracket, with zircons between 1600–2500 Ma making up ∼ 8% of the total population. The youngest components in two samples were 495 and 513 Ma. Di Vincenzo *et al.* (2014) recorded Ar–Ar detrital muscovite fusion ages mainly in the range 505–560 Ma, with a minimum mean age of 506 Ma. Samples of the Robertson Bay Group have a dominant late Panafrican detrital zircon population within the range *ca* 450–700 Ma) and a lesser Grenvillian population within the range 900–1300 Ma (Fioretti *et al.,* 2003, Adams *et al.,* 2014 and Estrada *et al.,* 2016) (Table 6). Estrada *et al.* (2016) recorded small age peaks within the range 1600–2500 Ma making up *ca* 9% of the total population. The youngest significant zircon populations are 485 Ma (Estrada *et al.,* 2016), 481 and 488 Ma (Fioretti *et al.,* 2003) and 512 Ma (Adams *et al.,* 2014), although the last authors pointed to grains between 408–491 Ma of questionable reliability. Estrada *et al.* (2016) also recorded small age peaks from 1600–2500 Ma (probably individual grains) making up *ca* 9% of the total population (Table 6). Analysis of single crystal detrital micas in the Robertson Bay Group produced ages mainly between 490–650 Ma (youngest ages being 489–493 Ma), with only 4 between 830–1120 Ma (Henjes-Kunst, 2003). The minimum mean age recorded by DiVincenzo *et al.* (2014) was 483 Ma (Table 6).

References

Adams, C. J., Bradshaw, J. D., & Ireland, T. R. (2014). Provenance connections between late Neoproterozoic and early Paleozoic sedimentary basins of the Ross Sea Region, Antarctica, southeast Australia and southern Zealandia. *Antarctic Science, 26*, 173–182.

Allibone, A. H., Cox, S. C., Graham, I. J., Smellie, R. W., Johnstone, R. D., Ellery, S. G., & Palmer, K. (1993). Granitoids of the Dry Valleys Area, Southern Victoria Land, Antarctica: Plutons, field relationships, and isotopic dating. *New Zealand Journal of Geology and Geophysics, 36*, 281–297.

Andersen, T. (2002). Correction of common Pb in U–Pb analyses that do not report ^{204}Pb. *Chemical Geology, 192*, 59–79.

Bizzarro, M., Baker, J. A., Haack, H., Ulfbeck, D., & Rosing, M. (2003). Early history of Earth's crust-mantle system inferred from hafnium isotopes in chondrites. *Nature, 421*, 931–933.

Black, L. P., & Gulson, B. L. (1978). The age of the Mud Tank carbonatite, Strangways Range, Northern Territory. *BMR Journal of Australian Geology and Geophysics,* 3, 227–232.

Blichert-Toft, J., Chauvel, C., & Albarède, F. (1997). The Lu–Hf geochemistry of chondrites and the evolution of the mantle–crust system. *Earth and Planetary Science Letter, 148*, 243–258, Erratum. *154*, 349.

Cooper, A. F., Maas, R., Scott, J. M., & Barber, A. J. W. (2011). Dating of volcanism and sedimentation in the Skelton Group, Transantarctic Mountains: Implications for the Rodinia–Gondwana transition in southern Victoria Land, Antarctica. *Geological Society of America Bulletin, 123*, 681–702.

Cook, Y. A., & Craw, D. (2001). Amalgamation of disparate crustal fragments in the Walcott Bay-Foster Glacier area, Southern Victoria Land, Antarctica. *New Zealand Journal of Geology & Geophysics, 44*, 403–416.

Curtis, M. L., Millar, I. L., Storey, B. C., & Fanning, C. M. (2004). Structural and geochronological constraints of early Ross orogenic deformation in the Pensacola Mountains, Antarctica. *Geological Society of America Bulletin, 116,* 619–636.

Di Vincenzo, G., Grande, A., & Rossetti, F. (2014). Paleozoic siliciclastic rocks from northern Victoria Land (Antarctica): Provenance, timing of deformation, and implications for the Antarctica–Australia connection. *Geological Society of America Bulletin, 126,* 1416–1438.

Estrada, S., Läufer, A., Eckelmann, K., Hofmann, M., Gärtner, A., & Linnemann, U. (2015). Continuous Neoproterozoic to Ordovician sedimentation at the East Gondwana margin — Implications from detrital zircons of the Ross Orogen in northern Victoria Land, Antarctica. *Gondwana Research, 37*, 426–448.

Fioretti, A. M., Black, L. P., Henjes-Kunst, F., & Visona, D. (2003). Detrital zircon age patterns from a large gneissic xenolith from Cape Phillips granite and from Robertson Bay Group metasediments, Northern Victoria Land, Antarctica. In D. K. Fütterer, D. Damaske, G. Kleinschmidt, H. Miller & F. Tessensohn (Eds.) *9th International Symposium on Antarctic Earth Sciences (ISAES IX) Antarctic Contributions to Global Earth Sciences, Programme and Abstracts* (pp. 94–95). Terra Nostra.

Fitzsimons, I. C. W. (2000). Grenville-age basement provinces in East Antarctica: evidence for three separate collisional orogens. *Geology, 28*, 879–882.

Goodge, J. W., Myrow, P., Phillips, D., Fanning, C. M., & Williams, I. S. (2004a). Siliciclastic record of rapid denudation in response to convergent-margin orogenesis, Ross Orogen, Antarctica. In M. Berne & C. Spiegel (Eds.) *Detrital Thermochronology — Provenance analysis, exhumation, and landscape evolution of mountain belts* (pp. 101–122). Geological Society of America Special Paper 378. Boulder, Colorado:

Goodge, J. W., Myrow, P., Williams, I., & Bowring, S. (2002). Age and provenance of the Beardmore Group, Antarctica: Constraints on Rodinia supercontinent breakup. *Journal of Geology*, *110*, 393–406.

Goodge, J. W., Williams, I. S., & Myrow, P. (2004b). Provenance of Neoproterozoic and lower Paleozoic siliciclastic rocks of the central Ross Orogen, Antarctica: Detrital record of rift-, passive- and active-margin sedimentation. *Geological Society of America Bulletin, 116*, 253–1279

Griffin, W. L., Belousova, E. A., Shee, S. R., Pearson, N. J., & O'Reilly, S. Y. (2004). Archean crustal evolution in the northern Yilgarn Craton: U–Pb and Hf-isotope evidence from detrital zircons. *Precambrian Research, 131*, 231–282.

Griffin, W. L., Pearson, N. J., Belousova, E. A., Jackson, S. R., Van Achterbergh, E., O'Reilly, S. Y., & Shee, S. R. (2000). The Hf isotope composition of cratonic mantle: LAM-MCICPMS analysis of zircon megacrysts in kimberlites. *Geochimica et Cosmochimica Acta, 64*, 133–147.

Griffin, W. L., Spetius, Z. V., Pearson, N. J., & O'Reilly, S. Y. (2002). In situ Re–Os analysis of sulfide inclusions in kimberlitic olivine: new constraints on depletion events in the Siberian lithospheric mantle. *Geochemistry, Geophysics, Geosystems, 3,* doi:10.1029/2001GC000287.

Griffin, W. L., Powell, W. J., Pearson, N. J., & O'Reilly, S. Y. (2008). GLITTER: data reduction software for laser ablation ICP-MS. In P. Sylvester (Ed.) *Laser ablation-ICP-MS in the Earth Sciences* (pp. 204–207). Mineralogical Association of Canada Short Course Series, 40, Appendix 2.

Hagen-Peter, G., Cottle, J. M., Smit, M., & Cooper, A. F. (2016). Coupled garnet Lu–Hf and monazite U–Pb geochronology constrain early convergent margin dynamics in the Ross orogen, Antarctica. *Journal of Metamorphic Geology, 34*, 293–319

Jackson, S. E., Pearson, N. J., Griffin, W. L., & Belousova, E.A. (2004). The application of laser ablation microprobe-inductively coupled plasma-mass spectrometry (LAM-ICPMS) to in situ U–Pb zircon geochronology. *Chemical Geology, 211*, 47–69.

Ludwig, K. R. (2003). *Isoplot 3.0. A Geochronological Toolkit for Microsoft Excel.* Berkeley Geochronology, Center Special Publication 4. 70 pp.

Meert, J. G. (2003). A synopsis of events related to the assembly of eastern Gondwana. *Tectonophysics, 362*, 1–40.

Millar, I. L., & Storey, B. C. (1995). Early Paleozoic rather than Neoproterozoic volcanism and rifting within the Transantarctic Mountains. *Journal of the Geological Society of London, 152*, 417–420.

Myrow, P. M., Pope, M. C., Goodge, J. W., Fischer, W., & Palmer, A. R. (2002). Depositional history of pre-Devonian strata and timing of Ross orogenic tectonism in the central Transantarctic Mountains, Antarctica. *Geological Society of America Bulletin, 114*, 1070–1088.

Paulsen, T. S., Encarnaci_on, J., Grunow, A. M., Valencia, V. A., Layer, P. W., Pecha, M., … Rasoazanamparany, C. (2015). Detrital mineral ages from the Ross Supergroup, Antarctica: Implications for the Queen Maud terrane and outboard sediment provenance on the Gondwana margin. *Gondwana Research, 27,* 377–391.

Rocchi, S., Bracciali, L., Di Vincenzo, G., Gemelli, M., & Ghezzo, C. (2011). Arc accretion to the early Paleozoic Antarctic margin of Gondwana in Victoria Land. *Gondwana Research, 19*, 594–607.

Rowell, A. J., Van Schmus, W. R., Storey, B. C., Fetter, A. H., & Evans, K. R. (2001). Latest Neoproterozoic to Mid-Cambrian age for the main deformation phases of the Transantarctic Mountains: New stratigraphic and isotopic constraints from the Pensacola Mountains, Antarctica. *Journal of the Geological Society of London, 158,* 295–308.

Scherer, E., Munker, C., & Mezger, K. (2001). Calibration of the Lutetium–Hafnium clock. *Science, 293*, 683–687.

Stump, E. (1995). The Ross Orogen of the Transantarctic Mountains. Cambridge: Cambridge University Press, 284 pp.

Stump, E., Gehrels, G., Talarico, F., & Carosi, R. (2007). Constraints from detrital zircon geochronology on the early deformation of the Ross orogen, Transantarctic Mountains, Antarctica. In A. K. Cooper & C. R. Raymond (Eds.), *Antarctica: A Keystone in a Changing World Antarctica: 4780 Abstract 166. Proceedings of the 10th ISAES.* US Geological Survey Open File Report 2007-1047. Retrieved from https://pubs.usgs.gov/of/2007/1047.

Wiedenbeck, M., Alle, P., Corfu, F., Griffin, W. L., Meier, M., Oberli, F., Von Quadt, A., Roddick, J. C., & Spiegel, W. (1995). Three natural zircon standards for U–Th–Pb, Lu–Hf trace element and REE analyses. *Geostandards Newsletter, 19*, 1–24.

Wysoczanski, R. J., & Allibone, A. H. (2004). Age, correlation, and provenance of the Neoproterozoic Skelton Group, Antarctica: Grenville age detritus on the margin of East Antarctica. *The Journal of Geology, 112,* 401–41.